JMEPEG (2006) 15:320-327
DOI: 10.1361/105994906X108585

1059-9495/$19.00

# TiC-Reinforced Cast Cr Steels

*Ö.N. Doğan, J.A. Hawk, and K.K. Schrems*

*(Submitted October 22, 2004; in revised form November 18, 2005)*

**A new class of materials, namely TiC-reinforced cast chromium (Cr) steels, was developed for applications requiring high abrasion resistance and good fracture toughness. The research approach was to modify the carbide structure of commercial AISI 440C steel for better fracture resistance while maintaining the already high abrasion resistance. The new alloys contained 12Cr, 2.5-4.5Ti, and 1-1.5C (wt.%) and were melted in a vacuum induction furnace. Their microstructure was composed primarily of a martensitic matrix with a dispersion of TiC precipitates. Modification of TiC morphology was accomplished through changing the cooling rate during solidification. Wear rates of the TiC-reinforced Cr steels were comparable to that of AISI 440C steel, but the impact resistance was much improved.**

**Keywords** cast steel, chromium steel, corrosion resistant steel, solidification of TiC-containing steel, titanium carbide precipitates, wear-resistant steel

## 1. Introduction

The search for materials with higher toughness and more wear and corrosion resistance continues unabated, as equipment manufacturers push components to their operating limits in terms of friction and wear. In environments where abrasion, corrosion, and impact are prevalent, research has shown that white cast irons (WCI) and steels with complex carbide networks do not perform well. Performance is associated with both matrix and carbides (primarily chromium-iron carbides). The morphology and distribution of carbides in WCI and steels are not well suited for many applications. Anisotropic properties, angular shape, interconnectedness, large size, and volume fraction of carbides have detrimental effects on toughness. In addition, these carbides are brittle and less hard (1200-1600 HV) than other types of carbides: for example, NbC (2400-2850 HV), VC (2460-3150 HV), and TiC (2000-3200 HV), to name just three.

The focus on using TiC as a strengthening and hardening phase in cast steels has been considerable during the last decade. There are essentially two ways to obtain a high volume fraction of TiC particles in an alloy: through melt solidification processing (M/S) (Ref 1-7) or via powder metallurgy processing techniques (P/M) (Ref 8-14). Additionally, TiC has been incorporated into the surface region of Fe-based alloys through surface remelting and laser cladding (Ref 15). These efforts have been driven by the fact that TiC is an extremely hard carbide; hence, the resultant composite is expected to possess high hardness and good wear resistance. For example, Chen et al. (Ref 16), using a pin-on-disk apparatus, showed that under low-stress abrasion conditions, Fe-TiC ($V_f = 0.22$) composites are more resistant to abrasion than WCI, which also form carbides and carbide colonies in situ from the melt.

**Ö.N. Doğan, J.A. Hawk,** and **K.K. Schrems,** Albany Research Center, U.S. Department of Energy, Albany, Oregon 97321. Contact e-mail: dogano@alrc.doe.gov.

More recently, Pagounis et al. (Ref 11-13) have studied the physical metallurgy and abrasion resistance of TiC-reinforced ($V_f = 0.05$-$0.30$) WCI (i.e., a Fe-26Cr-2C matrix) and the effect that different heat treatments have on matrix, composite hardness, and wear resistance. They also studied the effect of carbide size on wear. In general, they observed that the abrasive wear rate of the WCI composites decreased with increasing composite hardness, which is a consequence of carbide volume fraction and composite heat treatment. As the volume fraction of TiC increased, the hardness of the composite increased. In addition, high solutionizing temperatures tended to give a lower wear rate for equivalent volume fractions of TiC particles. It was also observed that TiC particle size influenced the abrasive wear rate in unidirectional scratching abrasion. At equivalent TiC particle volume fractions, the distribution of fine particles provided better wear resistance than did the coarse particles.

Wear of TiC-reinforced metal matrix composites produced using a liquid-phase sintering technique was investigated by the present authors (Ref 17). These composites contained a high volume fraction (0.35-0.45) of TiC particles. In a high-stress, multidirectional abrasive wear environment, larger TiC particles provided better protection for the soft matrices. In a low stress, unidirectional wear environment, it was more important to minimize the interparticle spacing to increase the wear resistance. In an earlier paper, the wear performance of these composites was compared with the cast chromium (Cr) steels with TiC reinforcement (Ref 18).

In this paper, development of TiC-reinforced cast Cr steels for wear-corrosion applications such as refiner plates and bearings is outlined. Solidification behavior and resulting microstructure of the cast TiC-reinforced Cr steels (Cr/TiC steels) is reported. These steels were tested under high-stress and low-stress abrasion, as well as under impact loading. The results are compared with mechanical behavior of an AISI type 440C steel.

## 2. Experimental Procedures

The cast steels with TiC reinforcement used in this work were melted in a vacuum induction furnace. Elemental metals were used to charge the furnace, except for Ti, which was

added as ferrotitanium. Chemical compositions were determined using an x-ray fluorescence technique, and the results are listed in Table 1. An AISI type 440C steel was used as a comparison material.

The microstructures of the steels were characterized using light optical microscopy, scanning electron microscopy (SEM), and x-ray diffraction (XRD). Image analysis was conducted using back-scattered electron images due to the large compositional contrast between matrix and carbides. TiC particle size was determined by measuring 16 Feret diameters per particle. The reported volume fraction of carbide particles is actually the area fraction of particles on the plain of polish. Ten images at 500× magnification were analyzed for each sample. At this magnification, one pixel represents 0.25 μm.

Thermal analysis was performed on an instrument fitted with a pair of matched alumina crucibles with tantalum lids. One crucible contained the sample, with a mass of approximately 0.25 g, while the other crucible was empty. After evacuation of the furnace chamber, a flow of 1.7 $cm^3$/s of high-purity argon was maintained throughout the experiment. Specimens were heated to approximately 1550 °C, allowed to equilibrate for 5 min, and then cooled to room temperature. Three different heating and cooling rates (1, 5, and 85 °C/min) were used. The temperature of the crucibles was monitored during heating and cooling.

The macrohardness values of the alloys were determined using both Rockwell C and Vickers (10 kg load) methods. A Vickers indenter was attached to an optical microscope and was used to determine the hardness of various microconstituents of the TiC reinforced cast Cr steels using a 10 g load. Impact testing was performed using standard Charpy specimens without the notch as per ASTM A 327M (Ref 19). Four specimens were tested for each alloy. Fracture energy was recorded. Average and standard deviation values were calculated.

The pin abrasion wear test (Ref 20, 21) involved the wear of the flat end of a cylindrical pin (6.35 mm diameter by 25 mm length) in contact with an abrasive cloth (garnet, alumina, and SiC in this case) on a large slowly rotating cylindrical drum. The test is two-body and high-stress and produces a multidirectional groove pattern on the wear surface of the pin. A dead weight loading system applied a 66.7 N load to the specimen except when the load was varied to study its effect on wear rate. To evaluate wear rate as a function of load, discrete values of normal force were used: 17.5, 29.6, 41.8, 54.1, and 66.7 N. Abrasive particles used in these tests were 150, 240, and 400 grit (average abrasive particle size is 100, 58, and 37 μm, respectively).

After a specimen break-in cycle of four revolutions, wear data were collected after five revolutions, equivalent in magnitude to a sliding distance of 8 m. Three tests were performed on each alloy under each condition. The mass loss of the sample was measured after each wear test with the average value used to calculate the wear rate in terms of volume loss per unit sliding distance, as shown in Eq 1 (densities were determined via the Archimedes technique).

$$W = \frac{\Delta m}{\rho L} \quad \text{(Eq 1)}$$

where $\Delta m$ is the mass loss for the sample in mg, $\rho$ is the density of cast iron mg/$mm^3$, and $L$ is the sliding distance in meters. Thus, the units of $W$ are in $mm^3$/m. The coefficient of variation (COV) depends on the abrasive particle size, applied load, and abrasive type. For example, on 150 grit garnet, the COV was ≤3.1% for all alloys at 66.7 N. On 150 grit alumina, the COV was ≤1.4% at 66.7 N, while on 150 grit SiC, it was ≤1.4% at 66.7 N. This is in part due to the nature of the abrasive. The garnet is a naturally occurring mineral with wide variation in mineral quality, while alumina and SiC are synthetic. The maximum COV (6.0%) occurred on the 400 grit SiC abrasive, with the majority of values <3% for all other test conditions.

## 3. Results and Discussion

### 3.1 Microstructure

Commercial AISI 440C steel contains about 8% (by volume) second-phase particles. In the as-cast 440C, $M_7C_3$ type carbides predominate where M is primarily Cr and Fe. These $M_7C_3$ carbides form during solidification as a eutectic phase (a mixture of $M_7C_3$ and austenite) after the formation of proeutectic austenite dendrites. Consequently, the eutectic phase surrounds the austenite dendrites. Most of the time, the carbides are large and interconnected. XRD also shows that some of austenitic phase in the as-cast 440C transforms to martensite upon cooling to room temperature. In addition to primary $M_7C_3$, heat-treated 440C contains secondary precipitates within the prior austenite dendrites. These precipitates are $M_{23}C_6$-type carbides, and they form during isothermal annealing at 1000-1050 °C. As a result of this heat treatment, Cr and C content of austenite is lowered. This causes the martensite start temperature to move above room temperature. Although more of the austenite transforms to martensite after this heat

**Table 1 Chemical compositions (wt.%) of cast Cr/TiC and 440C steels**

| | Cr | Ti | Mn | Mo | Si | Ni | C | Fe |
|---|---|---|---|---|---|---|---|---|
| W589 | 12.4 | 2.6 | 1.0 | 0.8 | 1.0 | … | 1.0 | Balance |
| W590 | 12.3 | 3.6 | 1.0 | 0.8 | 1.0 | … | 1.2 | Balance |
| W591 | 12.6 | 4.5 | 1.0 | 0.8 | 1.0 | … | 1.5 | Balance |
| W592 | 12.6 | 4.8 | 0.9 | 0.8 | 0.9 | … | 1.5 | Balance |
| 440C | 17.1 | … | 0.6 | 0.6 | 0.8 | 0.3 | 1.0 | Balance |

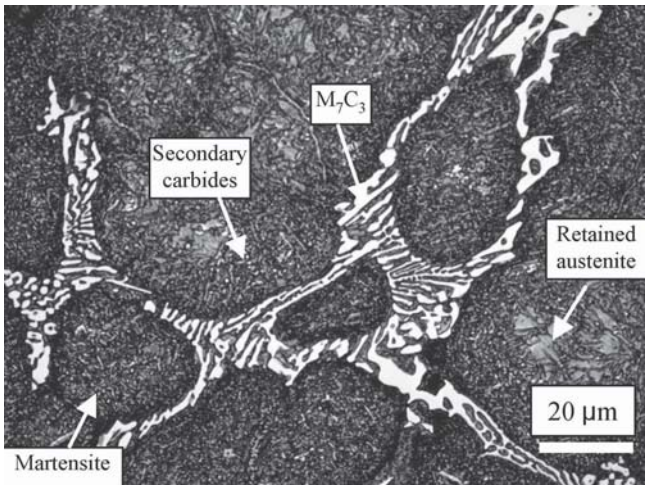


**Fig. 1** Optical micrograph of heat-treated AISI 440C, etched with Vilella's reagent

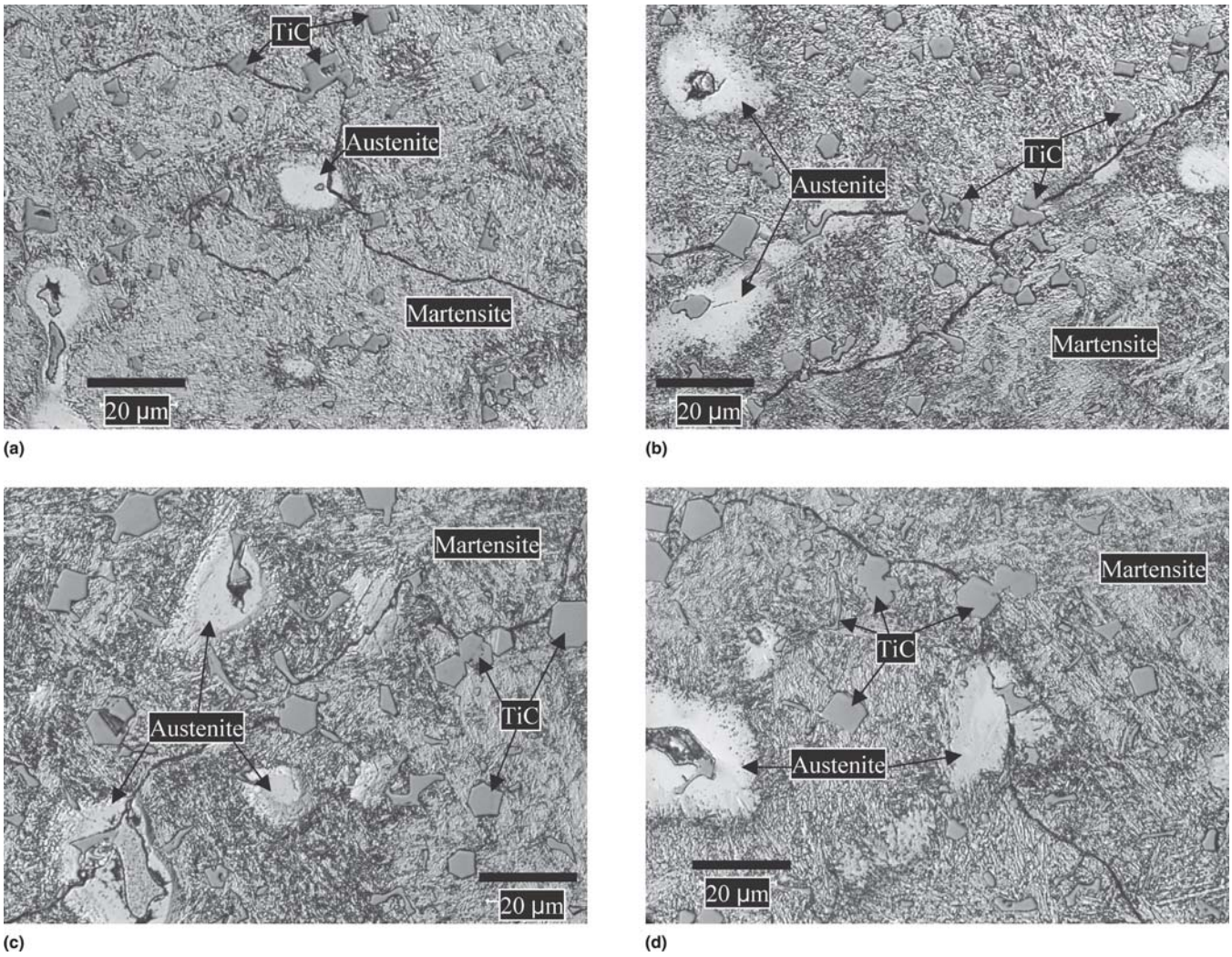


**Fig. 2** Optical micrographs of TiC reinforced Cr steels in as-cast condition, etched with Vilella's reagent: (a) 2.6Ti steel, (b) 3.6Ti steel, (c) 4.5Ti steel, and (d) 4.8Ti steel

**Table 2 Microstructural features of Cr/TiC steels**

| | TiC particle diameter, μm | | TiC volume fraction, % | | TiC interparticle spacing, μm | |
|---|---|---|---|---|---|---|
| **Materials** | **As-cast** | **Heat-treated** | **As-cast** | **Heat-treated** | **As-cast** | **Heat-treated** |
| W589 | 3.7 | 3.7 | 7.8 | 7.6 | 10.0 | 10.2 |
| W590 | 4.1 | 4.3 | 7.9 | 9.0 | 11.2 | 11.8 |
| W591 | 3.4 | 3.8 | 9.7 | 11.0 | 8.9 | 9.3 |
| W592 | 3.5 | 3.4 | 11.2 | 12.3 | 8.2 | 7.1 |

treatment, heat-treated 440C still contains a small amount of retained austenite. Because the primary $M_7C_3$ carbides in 440C are interconnected, particle size information was not acquired. Figure 1 illustrates the microstructure of 440C heat treated at 1000 °C for 1 h and air cooled.

XRD reveals that the cast Cr/TiC steels have a martensitic matrix in both the as-cast and heat-treated conditions. A small amount of austenite is present in the as-cast material. The majority of second-phase particles were determined to be TiC using both XRD and scanning electron microscopy (SEM)-wave-length dispersive x-ray spectroscopy (WDX). The TiC particles have a faceted cuboidal morphology (Fig. 2a-c) and are on average 3-4 μm in diameter in samples of the 2.6Ti, 3.5Ti, and 4.5Ti steels (Table 2 for details). The volume fraction of TiC particles increases from 7.6% in the 2.6Ti alloy to 12.3% in the 4.8Ti alloy. The TiC particles are uniformly dispersed throughout the matrix. The TiC particles in the 4.8Ti alloy, on the other hand, show two different morphologies. The large TiC particles are cuboidal while the smaller ones surrounding the large particles are elongated (Fig. 2d).

X-ray maps shown in Fig. 3 indicate that TiC precipitates contain a considerable amount of Mo and a small amount of Cr and Fe. This was confirmed by quantitative WDX analysis (Table 3). TiC in these alloys is slightly carbon deficient because the C content (about 47 at.%) is below its stoichiometric ratio.

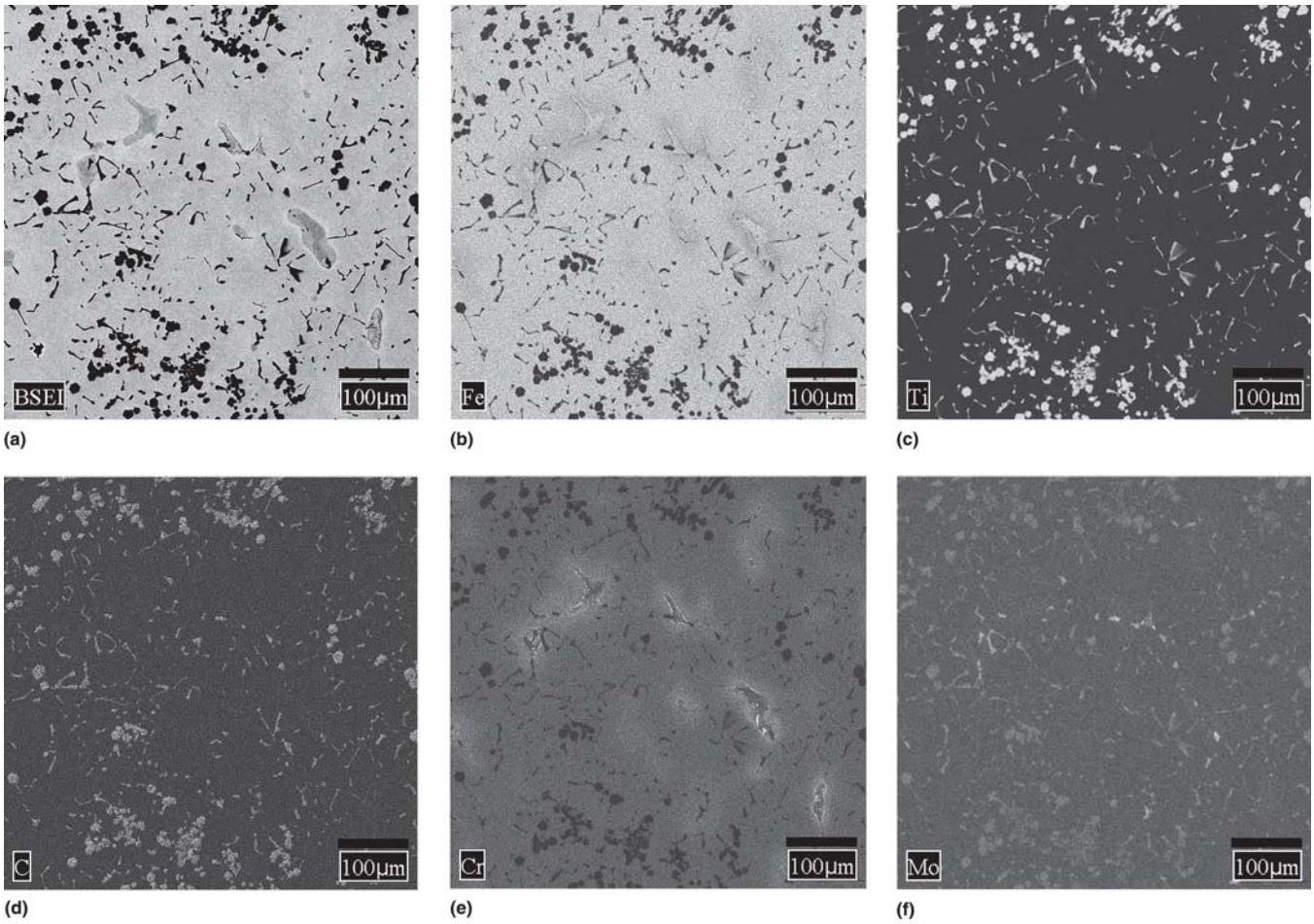


**Fig. 3** Back-scattered electron image (a) and x-ray maps (b-f) for various elements generated on the same area of the as-cast 4.8Ti steel, (b) Fe map, (c) Ti map, (d) C map, (e) Cr map, and (f) Mo map

**Table 3 Chemical compositions (wt.%) of various phases in W592 as determined using a wavelength-dispersive x-ray spectrometer attached to a scanning electron microscope**

| | C | Ti | Mo | Cr | Fe | Mn | Si |
|---|---|---|---|---|---|---|---|
| TiC | 18.45 | 77.56 | 5.01 | 1.33 | 1.16 | | |
| Austenite | 1.45 | 0.23 | 0.87 | 16.43 | 78.03 | 1.25 | 0.68 |
| Martensite | 1.30 | 0.31 | 0.61 | 13.34 | 85.80 | 0.98 | 0.96 |

Most of the Cr in the TiC-reinforced steels remains in the matrix as intended. For example, martensite in the as-cast W592 contains about 13 wt.% Cr while the retained austenite contains about 16.5 wt.% Cr (Table 3).

In the center of retained austenite grains is a region where small precipitates form. Because of the small size of these grains, the acquired WDX data may not accurately reflect the composition; therefore, they are not reported. Nevertheless, they are determined to be Fe- and Cr-rich carbides without Ti.

Examination of isopleths (Fig. 4) indicates that carbon concentrations less than a certain amount results in the permanent ferrite phase ($\alpha$) in the microstructure of these alloys. To obtain a fully martensitic matrix, the carbon concentration has to fall into the $\gamma$ + TiC phase field. To obtain a fully martensitic matrix in the as-cast microstructure, the minimum carbon concentrations in the 2.6Ti steel and 4.8Ti steel are 0.75 and 1.3 wt.%, respectively.

### 3.2 Solidification Reactions

Cooling curves and corresponding microstructures are shown in Fig. 5. On the bases of thermal analysis results, microstructures, and the equilibrium isopleths (Fig. 4), solidification paths may be proposed for the TiC-reinforced Cr steels. All compositions investigated in this study follow similar paths. They start freezing with formation of proeutectic TiC. These are the large, faceted particles distributed uniformly in the microstructure. The onset of this reaction is above 1500 °C (i.e., above the capability of the thermal analysis instrument), and as such, the thermal analysis results do not show this reaction. Next, the liquid composition goes through a monovariant eutectic reaction in which liquid freezes as ferrite and TiC ($L \rightarrow \alpha + TiC$). This reaction takes place at ~1400 °C. The remaining liquid then reacts with the ferrite phase to form austenite and TiC through a quasi peritectic reaction ($L + \alpha \rightarrow \gamma + TiC$). Another monovariant eutectic reaction ($L \rightarrow \gamma + TiC$) follows the peritectic reaction. This is the other major peak in the differential thermal analysis (DTA) curve that appears at ~1370 °C. Finally, the remaining liquid solidifies through another eutectic reaction ($L \rightarrow \gamma + TiC + M_7C_3$).

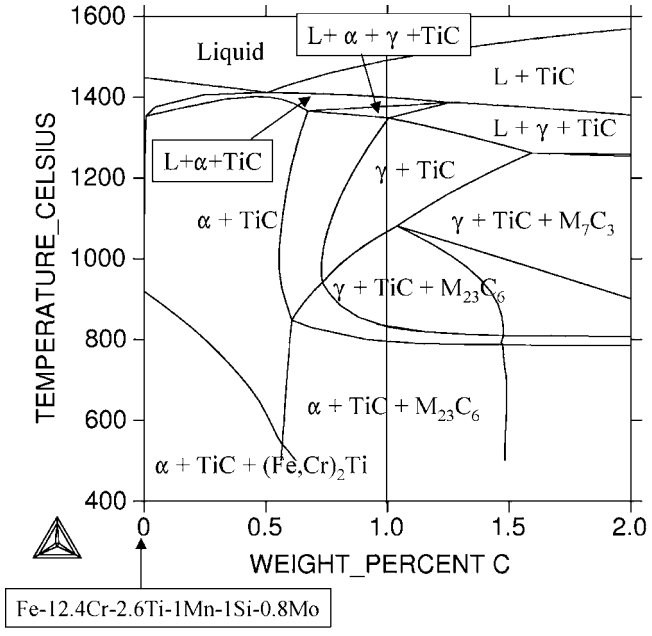


**Fig. 4** (a) Isopleths of 2.6Ti and (b) 4.8Ti alloys calculated using Thermocalc software with TCFE3 database

To investigate the effect of cooling rate and degree of undercooling on morphology of TiC particles, solidification experiments were conducted using a thermal analysis instrument. Increasing cooling rates resulted in increasing undercooling as well as significantly different morphologies for the TiC phase. For example, the monovariant eutectic reaction ($L \rightarrow \gamma + TiC$) in the 2.6Ti alloy occurs at 1383 °C at a cooling rate of 1 °C/min. Increasing the cooling rate to 5 °C/min lowers the temperature of this reaction to 1376 °C. At a cooling rate of 85 °C/min, this reaction takes place at 1344 °C.

The thermal analysis samples of TiC-reinforced steels cooled at three different rates resulted in very different eutectic TiC morphologies (Fig. 5). At a cooling rate of 1 °C/min, the eutectic TiC is generally in the form of coarse platelets within the eutectic cells. The eutectic cell structure is more pronounced at a cooling rate of 5 °C/min. Also, TiC particles are much smaller at this cooling rate in all of the alloys. At the highest cooling rate of 85 °C/min, a homogeneous dispersion of fine TiC particles dominates the microstructure. These fine TiC particles are much more isotropic than those formed at slower cooling rates. The ingots made by melting in induction furnace and solidifying in graphite molds had a microstructure that closely resembled the microstructure of thermal analysis samples solidified using the rapid cooling rate (85 °C/min).

### 3.3 Microhardness and Macrohardness

The micrograph in Fig. 6 shows the approximate hardness of various microconstituents in a segregated region that solidified last in the as-cast 2.6Ti steel. The martensitic matrix has a hardness of about 608 HV, while the retained austenite is much softer (~377 HV). The indents made on the $M_3C$ phase indicated a hardness of ~1760 HV. (The hardness values measured on the small phases should be used with caution and taken as very approximate values.)

Overall hardness of these materials is given in Table 4 for the as-cast and heat-treated conditions. The heat treatment used increases the hardness of AISI 440C steel dramatically, whereas it does not affect the hardness of TiC-reinforced Cr steels significantly. Although the heat treatment transforms a large amount of austenite present in the as-cast 440C to martensite, it transforms only a very small amount of retained austenite present in the TiC-Cr steels.

### 3.4 Impact Resistance

As shown in Fig. 7, modification of carbide structure of the steel improved the fracture energy significantly. All materials were tested in the heat-treated condition. The low fracture energy of the 440C steel is attributed to the interconnected network of the brittle $M_7C_3$ phase. Replacing this phase with even harder but more compact shaped and disconnected small TiC particles improved the fracture energy.

### 3.5 Wear Resistance

The results of the pin abrasion tests performed under different abrasive conditions for the Cr/TiC steels and 440C are summarized in Fig. 8-10. Wear rates on three different abrasive papers (garnet, alumina, and SiC) are shown in Fig. 8. For all alloys tested, a similar ranking of alloy wear rate was observed for each abrasive type. Harder abrasives caused higher wear rates in all materials. The rate of increase in wear rates of the Cr/TiC steels with increasing abrasive hardness was higher than that of the 440C steels. All TiC-reinforced Cr steels performed better than the heat-treated 440C on the garnet abrasive. On the alumina and SiC abrasives, the Cr/TiC steels had lower wear rates than the heat-treated 440C on the alumina and similar wear rates on the SiC. The wear rates of the Cr/TiC steels spread out to a larger range on the garnet abrasive. As the abrasive hardness increased, this range became smaller.

Figure 9 shows how the wear rates of all of the alloys varied as a function of SiC abrasive particle size. As expected, wear rate increased as abrasive particle size increased. Although all of the steels tested adhered to this trend, the wear rate of 440C steel increased linearly with increasing SiC size. On the other

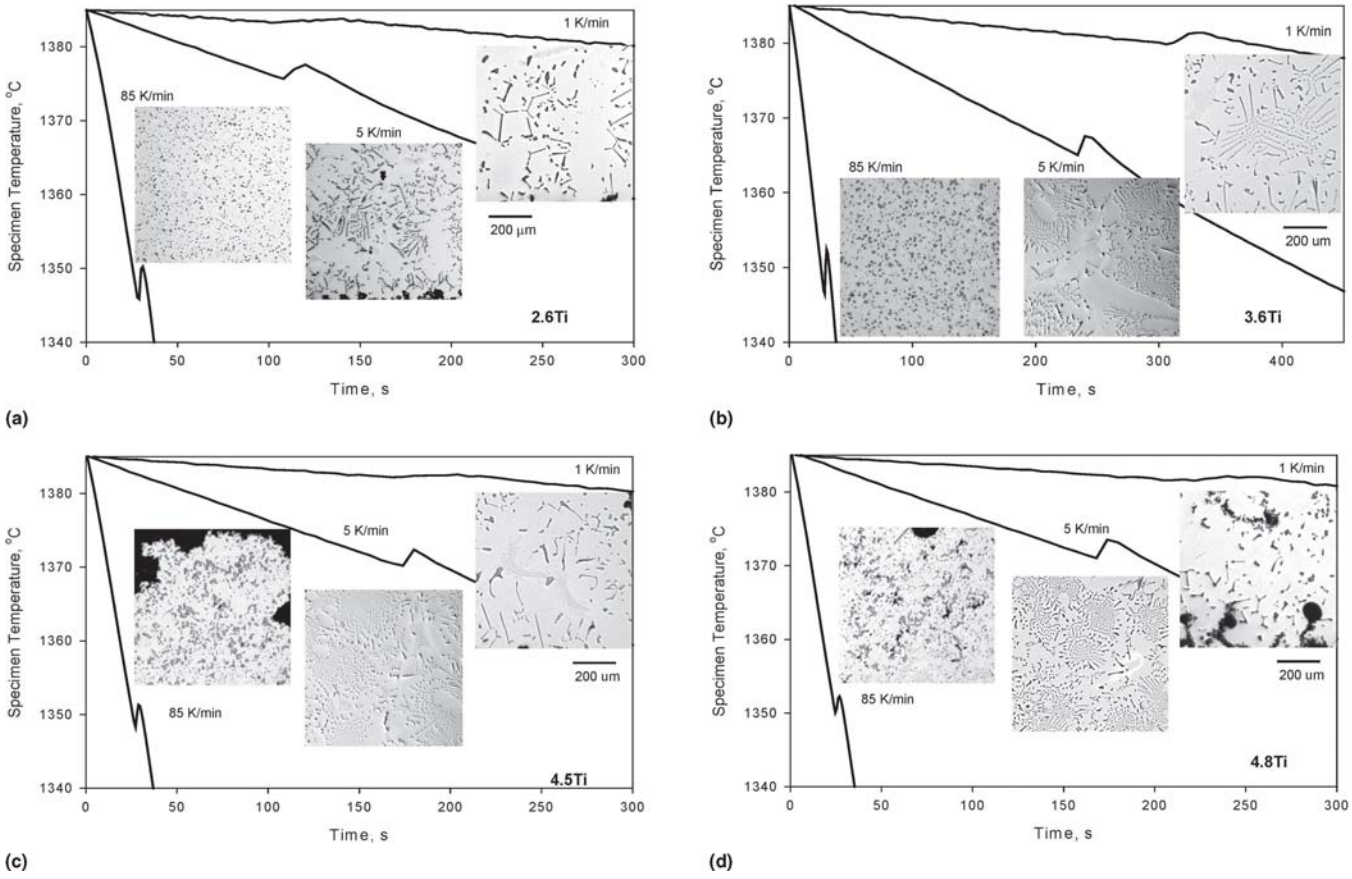


**Fig. 5** Cooling curves showing the formation of eutectic phase (γ+TiC) during solidification at three different cooling rates and resulting TiC morphology in (a) 2.6Ti alloy, (b) 3.6Ti alloy, (c) 4.5Ti alloy, and (d) 4.8Ti alloy

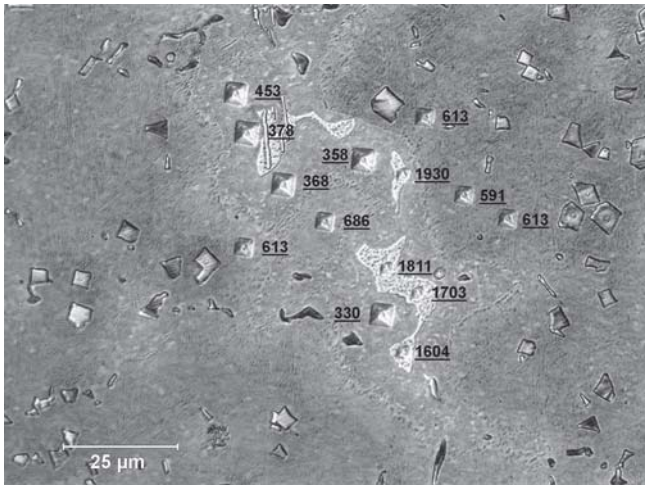


**Fig. 6** Microhardness values (Vickers) obtained on different phases on the 2.6Ti alloy

hand, the wear rates of Cr/TiC steels did not follow a linear trend as a function of abrasive size. As shown in Fig. 9, the average wear rate of the Cr/TiC steels was higher than the 440C steel with the 100 μm SiC. As the abrasive particle size was reduced, the average wear rate of the Cr/TiC steels became lower at a faster rate than that of 440C steel. With the 37 μm SiC, most Cr/TiC steels showed better wear resistance than 440C steel. These results suggest that the Cr/TiC steels may be a better choice of material than 440C steel for applications involving fine particles under abrasive wear conditions.

**Table 4 Hardness values of as-cast and heat-treated steels in Rockwell C and Vickers (kg mm$^{-2}$) scales**

| | As-cast | | Heat-treated | |
|---|---|---|---|---|
| **Materials** | **HRC** | **DPH** | **HRC** | **DPH** |
| W589 | 58.9 | 657 | 58.5 | 660 |
| W590 | 57.6 | 664 | 59.8 | 689 |
| W591 | 57.9 | 671 | 59.9 | 704 |
| W592 | 57.7 | 653 | 59.7 | 655 |
| 440C | 34.6 | 331 | 54.9 | 614 |

Figure 10 illustrates the effect of load on the wear rates of the 2.6Ti alloy, 4.5Ti alloy, and 440C (for the HT condition only) on 100 μm garnet. The general trend is for the wear rate to increase linearly with increasing load. The wear rate at each load was the lowest for the 4.5Ti steel. The rate of increase in the wear rate with load was also the lowest for this steel.

## 4. Summary

A new class of wear- and impact-resistant steels was developed using TiC precipitates (8-12 vol.%) as the strengthening phase in a high-Cr martensitic matrix. The cooling rate during solidification determines the morphology of TiC precipitates.

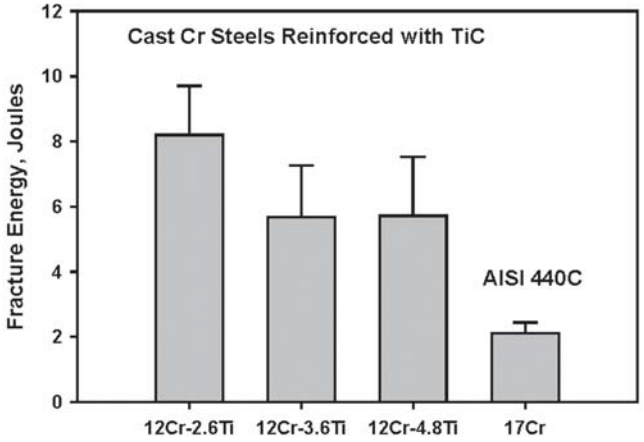


**Fig. 7** Impact resistance of the cast Cr-TiC steels compared with that of AISI 440C steel; error bars indicate the positive standard deviation

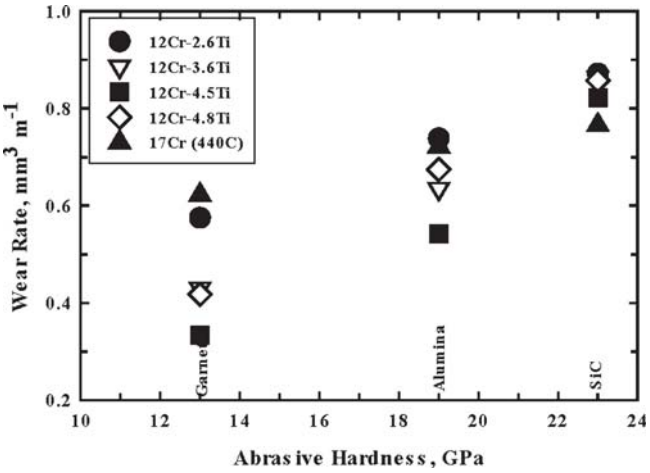


**Fig. 8** Wear rates of the cast Cr-TiC steels and AISI 440C steel measured using pin abrasion test on different abrasives

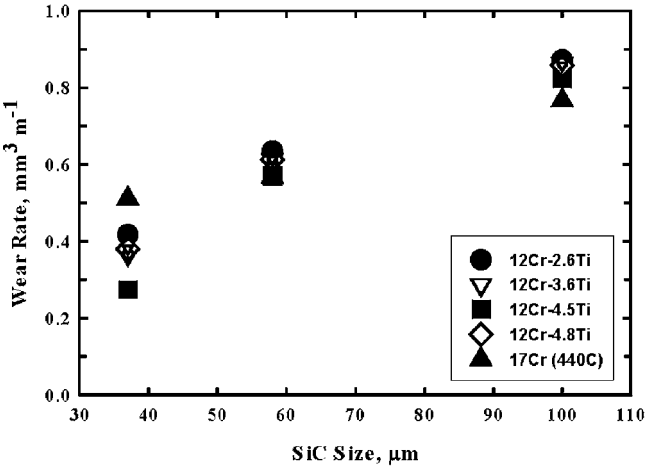


**Fig. 9** Wear rates of the cast Cr-TiC steels and AISI 440C steel as a function of abrasive size

At high cooling rates, TiC precipitates grow as compact and more isotropic shapes and form a fine dispersion throughout the matrix.

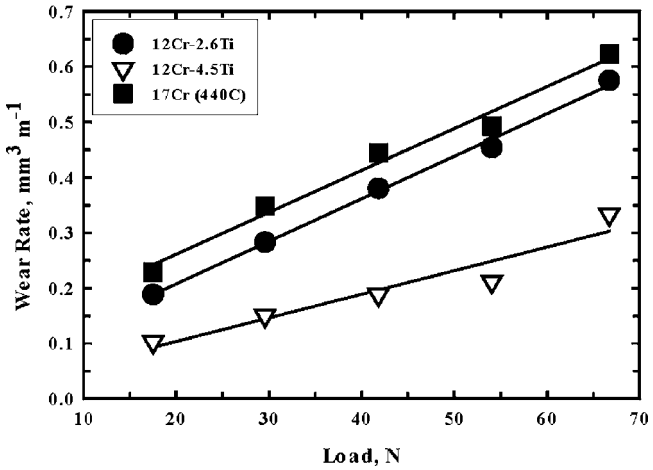


**Fig. 10** Wear rates of the cast Cr-TiC steels (heat treated) and AISI 440C (heat treated) steel as a function of load

Although the Cr/TiC steels have lower wear rates on less hard abrasives and finer SiC, the as-cast 440C possesses lower wear rates on the harder and coarser abrasives as determined using the pin abrasion test.

The low fracture energy of the 440C steel is attributed to the interconnected network of brittle $M_7C_3$ phase. Replacing this phase with even harder but more compact-shaped and smaller disconnected TiC particles improved the fracture energy.

## Acknowledgments

The authors thank Dale Govier for x-ray diffraction and x-ray fluorescence, Paul Danielson for metallography, Ed Argetsinger for vacuum melting, Marisa Arnold for thermal analysis, Ken Williamson for image analysis, Neal Duttlinger for impact tests, and Darrel Hoskins for pin abrasion tests.

## References

1. B.S. Terry and O.S. Chinyamakobvu, Dispersion and Reaction of TiC in Liquid Iron Alloys, *Mater. Sci. Technol.,* 1992, **8,** p 399-405
2. B.S. Terry and O.S. Chinyamakobvu, Effects of Cooling Rate and Heat Treatment on the Microstructure of Iron-Based Titanium Carbide Composites, *J. Mater. Sci.,* 1992, **27,** p 5666-5670
3. T.Z. Kattamis and T. Suganuma, Solidification Processing and Tribological Behavior of Particulate TiC-Ferrous Matrix Composites, *Mater. Sci. Eng.,* 1990, **A128,** p 241-252
4. B.V. Chambers, T.Z. Kattamis, J.A. Cornie, and M.C. Flemings, Solidification Behavior of Particulate TiC-Ferrous Matrix Composites, *Proc. Conf. on Solidification Processing,* J. Beech and H. Jones, Ed., Institute of Metals, London, 1987, p 435-438
5. Ö.N. Doğan and J.A. Hawk, Abrasion Resistance of in Situ Fe-TiC Composites, *Scripta Metall. Mater.,* 1995, **33,** p 953-958
6. Ö.N. Doğan and J.A. Hawk, Microstructure and Abrasion Resistance of Fe-TiC-$M_7C_3$ Composite, *Microstructural Science,* Vol 23, ASM International, 1996, p 251-257
7. C. Raghunath, M.S. Bhat, and P.K. Rohatgi, In Situ Technique for Synthesizing Fe-TiC Composites, *Scripta Metall. Mater.,* 1995, **32,** p 577-582
8. K.-W. Chae, D.-I. Chun, D.-Y. Kim, Y.-J. Baik, and K.-Y. Eun, Microstructural Evolution during the Infiltration Treatment of Titanium Carbide-Iron Composite, *J. Am. Ceram. Soc.,* 1990, **73,** p 1979-1982
9. B.K. Lograsso and R.M. German, Liquid Phase Sintered Titanium Carbide-Tool Steel Composites for High Temperature Service, *Progress in Powder Metallurgy,* Vol 43, MPIF, Princeton, NJ, 1987, p 415-439

10. Ö.N. Doğan, D.E. Alman, and J.A. Hawk, Wear Resistant, Powder Processed in Situ Iron-Matrix TiC Composites, *Advances in Powder Metallurgy and Particulate Materials,* MPIF, Princeton, NJ, 1996, p 83-97
11. E. Pagounis, M. Talvitie, and V.K. Lindroos, Influence of Reinforcement Volume Fraction and Size on the Microstructure and Abrasion Wear Resistance of Hot Isostatic Pressed White Iron Matrix Composites, *Metall. Mater. Trans. A,* 1996, **27A,** p 4171-4181
12. E. Pagounis, E. Haimi, J. Pietikainen, M. Talvitie, S. Vahvaselka, and V.K. Lindroos, Effect of Thermal Expansion Coefficients on the Martensitic Transformation in a Steel Matrix Composite, *Scripta Mater.,* 1996, **34,** p 407-413
13. E. Pagounis, M. Talvitie, and V.K. Lindroos, Influence of Matrix Structure on the Abrasion Wear Resistance and Toughness of a Hot Isostatic Pressed White Iron Matrix Composite, *Metall. Mater. Trans. A,* 1996, **27A,** p 4183-4191
14. S.E. Tarkan and M.K. Mal, "Machinable Carbides for High Performance Tooling and Wear Parts," Paper MR 73-927, presented at Society of Manufacturing Engineers, Dearborn, MI, 1973
15. N. Axén and K.-H. Zum Gahr, Abrasive Wear of TiC-Steel Composite Clad Layers on Tool Steel, *Wear,* 1992, **157,** p 189-201
16. M. Chen, T.Z. Kattamis, B.V. Chambers, and J.A. Cornie, Processing and Abrasive Wear Resistance of Cast TiC-Ferrous Matrix Particulate Composites, *Engineered Materials for Advanced Friction and Wear Applications,* ASM International, 1988, p 63-69
17. Ö.N. Doğan, J.A. Hawk, J.H. Tylczak, R.D. Wilson, and R.D. Govier, Wear of Titanium Carbide Reinforced Metal Matrix Composites, *Wear,* 1999, **225-229,** p 758-769
18. Ö.N. Doğan, J.A. Hawk, and J.H. Tylczak, Wear of Cast Chromium Steels with TiC Reinforcement, *Wear,* 2001, **250,** p 462-469
19. "Standard Test Methods for Impact Testing of Cast Irons," A327M-91, *Annual Book of ASTM Standards,* Vol. 01.02, ASTM, 2003
20. R. Blickensderfer and G. Laird II, A Pin-on-Drum Abrasive Wear Test and Comparison with Other Pin Tests, *J. Test. Eval.,* 1988, **16,** p 516-526
21. R. Blickensderfer, J.H. Tylczak, and B.W. Madsen, Laboratory Wear Testing Capabilities of the Bureau of Mines, *Bur. Mines Inf. Circ.,* 1985, p 22-25